Examination on a Criterion for a Debonding Fracture of Single Lap Joints from the Intensity of Singular Stress Field

Tatsujiro Miyazaki[1,*], **Nao-Aki Noda**[2], **Rong Li**[3], **Takumi Uchikoba**[3] **and Yoshikazu Sano**[2]

[1] Department of Mechanical Engineering Systems, University of the Ryukyus, 1 Senbaru, Nishihara-cho, Nakagami-gun, Okinawa 903-0213, Japan
[2] Department of Mechanical Engineering, Kyushu Institute of Technology, 1-1 Sensui-cho, Tobata-ku, Kitakyushu-shi, Fukuoka, 804-8550, Japan
[3] Department of Mechanical and Control Engineering, Graduate School of Engineering, Kyushu Institute of Technology, 1-1 Sensui-cho, Tobata-ku, Kitakyushu-shi, Fukuoka, 804-8550, Japan

* Corresponding author: t-miya@tec.u-ryukyu.ac.jp

Abstract In this study, the experimental adhesive strength is newly considered in terms of the singular stress appearing at the end of interface between the adhesive and adherent. Here the critical intensity of singular stress field is examined as the debonding criterion for all types of single lap joints under different adhesive thickness and overlap length. The intensity of singular stress can be evaluated by the application of the finite element method focusing on the stress value at the end element of the interface. It should be noted that except for the case of small overlap length the separation always occurs at the edge of the interface causing unstable growth and final brittle fracture. In this type of fracture it is found that the critical intensity of the stress singular field is constant independent of the adhesive thickness and overlap length.

Keywords Adhesion, Interface, Intensity of Singular Stress, Finite Element Method

1. Introduction

The requirements to packaging technology of semiconductors diversify with the miniaturization and high-performance of the electronics [1, 2]. The packages of semiconductors contain many various interfaces. For example, the connection of the semiconductor to the substrate, resin seal of semiconductor, multilayer structures composed of the dissimilar semiconductor materials. In order to ensure the reliability of the packages of semiconductors, the method for evaluating the debonding fracture strength properly is required [3 - 5]. Generally, the debonding strength of the dissimilar material joints depends on the material combination, load condition, adhesive condition and so on. Because the experimental evaluation of the adhesive strength is time-consuming job, the practical and convenient debonding fracture criterion and evaluation method are asked for.

Recently, the authors examined the experimental data for the butt joints of medium carbon steel bonded by epoxy resin under various adhesive thicknesses [6]. The debonding fracture criterion can be described by the constant value of the critical intensity of the singular stress field at the fracture, $K_{\sigma c}$, independent of the adhesive thickness [7]. When the joint is satisfied with the small scale yielding condition, the adhesive strength is predicted accurately by the debonding fracture criterion based on the intensity of the singular stress field [8, 9]. In this study, the debonding criterion for all types of single lap joints (SLJs) will be discussed under various adhesive thickness and overlap length in terms of the critical intensity of singular stress field as $K_{\sigma c}$ = constant. The recent experimental results performed on SLJs by Park *et al* [10] will be used. In this experiment, Park *et al* evaluated the damage zone size at fracture while considering the non-linear deformation behavior of the adhesive and adherent. Although the various methods were examined, the debonding fracture criterion cannot be expressed simply and conveniently [11, 12].

2. Experimental results of single lap joint

In this study, the experimental results obtained by Park *et al* [10] will be used in order to examine the validation of evaluation method of the adhesive strength. In the experiments, Aluminum alloy 6061-T6 and epoxy resin were used as adherent and adhesive, respectively. Table 1 shows the mechanical properties of the adherent and adhesive. Figure 1 shows the specimen configuration. Table 2 and Figure 2 show the experimental tensile adhesive strength P_{af}. As for all specimens except for specimen A10, the relation between the load and displacement is almost linear. Therefore, it can be considered that the fractures were caused by the unstable growth of the interfacial debonding crack which was initiated from the corner edge. The results bring the validation of the evaluation based on the intensity of the singular stress field. When the overlap length becomes long under constant adhesive thickness condition, the adhesive strength tends to increase; when the adhesive layer becomes thick under constant overlap length, the adhesive strength does not change remarkablely. Figure 3 shows the average shear stress at the fracture, τ_c. When l_2 is smaller than about 15mm, the τ_c becomes constant at about 28.3MPa. However, when l_2 is larger than about 15mm, the τ_c tends to decrease. The fracture is caused by the general yielding of the adhesive layer when the overlap length is small enough; in this case, the τ_c becomes constant. In this study, it is supposed that the cohesive fracture occurs when l_2 < 15mm and the adhesive fracture occurs when l_2 > 15mm. Therefore, although the fracture criterion for SLJ having small overlap length can be described by the average shear stress at the fracture, that for SLJ having long overlap length cannot be described by the stress.

Table 1 Material properties [10)]

Material	E [GPa]	ν
Adherent 6061-T6	68.9	0.30
Adhesive Epoxy resin	4.2	0.45

E : Young's modulus, ν : Poisson ratio

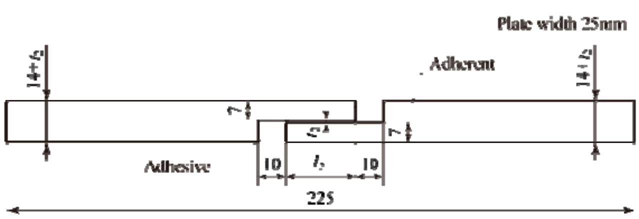

Figure 1 Specimen configurations [10)]

Table 2 Experimental tensile adhesive strength by Park *et al* [10)]

(a) t_2 = constant condition

Specimen	l_2 [mm]	t_2 [mm]	P_{af} [kN]
A10	10	0.15	6.87
A15	15	0.15	10.57
A20	20	0.15	12.41
A25	25	0.15	14.17
A30	30	0.15	14.56
A35	35	0.15	16.41
A40	40	0.15	18.09
A50	50	0.15	18.22

(b) l_2 = constant condition

Specimen	l_2 [mm]	t_2 [mm]	P_{af} [kN]
A25	25	0.15	14.17
A25-30	25	0.30	14.32
A25-45	25	0.45	14.26
A25-90	25	0.90	14.19
A30	30	0.15	14.56
A30-30	30	0.30	16.91
A30-45	30	0.45	16.12
A30-90	30	0.90	15.37

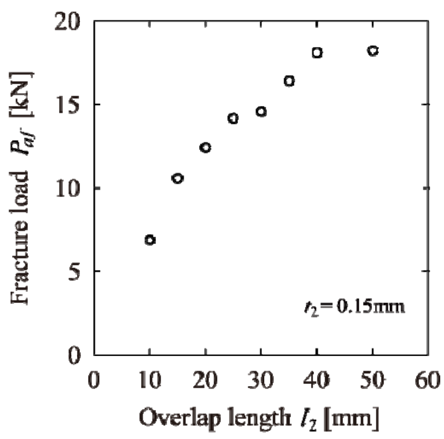

(a) t_2 = constant condition

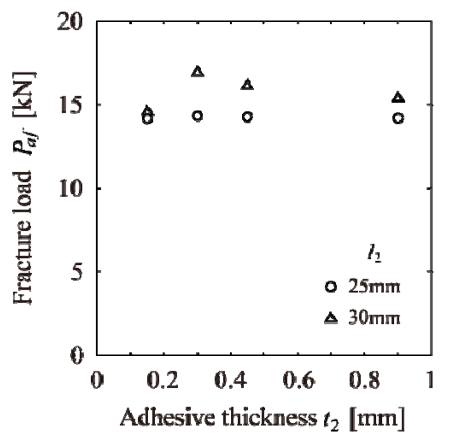

(b) l_2 = constant condition

Figure 2 Experimental adhesive strength P_{af} [10)]

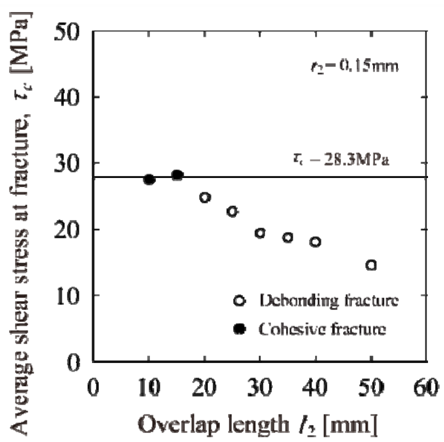

Figure 3 Average shear stress at fracture of specimens with t_2 = 0.15 mm [10)]

3. Analysis

3.1. Analysis model and method

Figure 4 shows the schematic illustration of the analysis model. Dundurs' parameters at point O are α = -0.8699 and β = -0.06642. The order of stress singularity is two different real values λ_1 = 0.6062 and λ_2 = 0.9989. When the eigenvalue equation has two different real roots, the stresses at a distance r on the interface from the corner edge O can be expressed as follows.

$$\sigma_y = \frac{K_{\sigma 1}}{r^{1-\lambda_1}} + \frac{K_{\sigma 2}}{r^{1-\lambda_2}}, \quad \tau_{xy} = \frac{K_{\tau 1}}{r^{1-\lambda_1}} + \frac{K_{\tau 2}}{r^{1-\lambda_2}} \tag{1}$$

Here, σ_y is the stress in the y direction, τ_{xy} is the shear stress.

In this analysis, the method proposed by Noda *et al* [13] is used. In this analysis, the elements near the edge corners of all models were set so as to be same size and shape. And then, minimum size of the element at the edge corner, $e_{\min}$, is changed, the influence of the mesh pattern on the stress distribution is investigated. The $e_{\min}$ value is set to 3^{-8}, 3^{-9}, 3^{-10} and 3^{-11}.

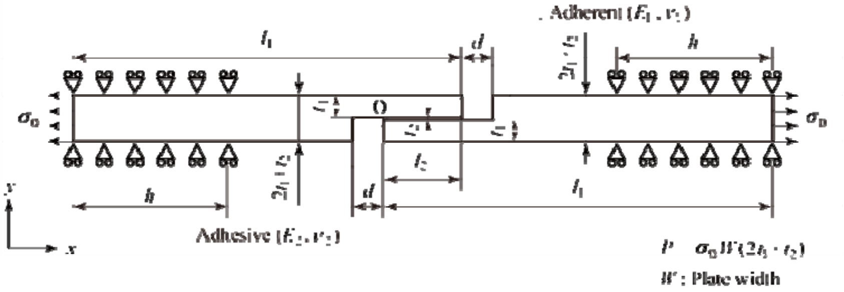

Figure 4 Analysis model and boundary condition

3.2. Characteristics of singular stress field at the edge corner

The characteristics of the singular stress field at the corner edge are mentioned using the analysis results of the specimens A25, A50 and A25-90. Figure 5 shows the relationship between the $\sigma^{\mathrm{A50}}_{y,FEM}/\sigma^{\mathrm{A25}}_{y,FEM}$, $\tau^{\mathrm{A50}}_{xy,FEM}/\tau^{\mathrm{A25}}_{xy,FEM}$ and r under the applied stress σ_0 = 1MPa. Then, Figure 6 shows the relationship between the $\sigma^{\mathrm{A50}}_{y0,FEM}/\sigma^{\mathrm{A25}}_{y0,FEM}$, $\tau^{\mathrm{A50}}_{xy0,FEM}/\tau^{\mathrm{A25}}_{xy0,FEM}$ and e_{min}. When t_2 are set constant, the stress ratios almost become constant independent of e_{min}. Figure 7 shows the relationship between the $\sigma^{\mathrm{A25–90}}_{y,FEM}/\sigma^{\mathrm{A25}}_{y,FEM}$, $\tau^{\mathrm{A25\text{-}90}}_{xy,FEM}/\tau^{\mathrm{A25}}_{xy,FEM}$ and r under the applied stress σ_0 = 1MPa. Then, Figure 8 shows the relationship between the $\sigma^{\mathrm{A25\text{-}90}}_{y0,FEM}/\sigma^{\mathrm{A25}}_{y0,FEM}$, $\tau^{\mathrm{A25–90}}_{xy0,FEM}/\tau^{\mathrm{A25}}_{xy0,FEM}$ and e_{min}. The stress distributions of the specimen A25-90 are different from those of the specimen A50. That is because the moment which is applied to the adhesive layer changes depending on the adhesive thickness. However, when the r is smaller than about 10^{-4} mm, the $\sigma^{\mathrm{A25\text{-}90}}_{y0,FEM}/\sigma^{\mathrm{A25}}_{y0,FEM}$ and $\tau^{\mathrm{A25–90}}_{xy,FEM}/\tau^{\mathrm{A25}}_{xy,FEM}$ almost become constant. Then, the stress ratios at the edge corner, $\sigma^{\mathrm{A25\text{-}90}}_{y,FEM}/\sigma^{\mathrm{A25}}_{y,FEM}$ and $\tau^{\mathrm{A25–90}}_{xy0,FEM}/\tau^{\mathrm{A25}}_{xy0,FEM}$, become constant independent of the e_{min}. From the results, the stresses on the interface near the corner edge are expressed with as follows independent of the t_2 and l_2.

$$\sigma_y = \frac{K_{\sigma 1}}{r^{1-\lambda_1}} + \frac{K_{\sigma 2}}{r^{1-\lambda_2}} \cong K_\sigma \left(\frac{1}{r^{1-\lambda_1}} + \frac{C_\sigma}{r^{1-\lambda_2}} \right), \tag{2}$$

$$\tau_{xy} = \frac{K_{\tau 1}}{r^{1-\lambda_1}} + \frac{K_{\tau 2}}{r^{1-\lambda_2}} \cong K_\tau \left(\frac{1}{r^{1-\lambda_1}} + \frac{C_\tau}{r^{1-\lambda_2}} \right) \tag{3}$$

Here, C_σ and C_τ are constant. The intensities of singular stress field of the reference problem and the unknown problem are denoted with K_σ and K^*_σ, respectively. Then, the stresses in the y direction at the edge corner of the unknown problem and the reference problem, which are obtained from the FEM analysis, are denoted with $\sigma_{y0,FEM}$ and $\sigma^*_{y0,FEM}$, respectively. From Equation (2), the relation between K_σ / K^*_σ and $\sigma_{y0,FEM}/\sigma^*_{y0,FEM}$ can be expressed as follows.

$$\frac{K_\sigma}{K^*_\sigma} = \frac{\sigma_{y0,FEM}}{\sigma^*_{y0,FEM}} \tag{4}$$

If the K^*_σ has been solved, the $\sigma_{y0,FEM}$ is equivalent with the K_σ because the $\sigma^*_{y0,FEM}$ can be obtained from the FEM analysis of the reference problem. The $\tau_{xy0,FEM}$ is also equivalent with the K_τ .

As shown in Figure 6, it is found that the different between $\sigma^{\mathrm{A50}}_{y0,FEM}/\sigma^{\mathrm{A25}}_{y0,FEM}$ and $\tau^{\mathrm{A50}}_{xy0,FEM}/\tau^{\mathrm{A25}}_{xy0,FEM}$ tends to become small with the r decreasing. Then, from Figure 8, the different between $\sigma^{\mathrm{A25\text{-}90}}_{y0,FEM}/\sigma^{\mathrm{A25}}_{y0,FEM}$ and $\tau^{\mathrm{A25\text{-}90}}_{xy0,FEM}/\tau^{\mathrm{A25}}_{xy0,FEM}$ tends to become small with the r decreasing. From Figures 6 and 8, the relations of $\sigma^{\mathrm{A50}}_{y0,FEM}/\sigma^{\mathrm{A25}}_{y0,FEM} = \tau^{\mathrm{A50}}_{xy0,FEM}/\tau^{\mathrm{A25}}_{xy0,FEM}$ and $\sigma^{\mathrm{A25\text{-}90}}_{y0,FEM}/\sigma^{\mathrm{A25}}_{y0,FEM} = \tau^{\mathrm{A25\text{-}90}}_{xy0,FEM}/\tau^{\mathrm{A25}}_{xy0,FEM}$ can be confirmed. This means $\sigma_{y0,FEM}/\sigma^*_{y0,FEM} = \tau_{xy0,FEM}/\tau^*_{xy0,FEM}$, that is, following equation.

$$\frac{K_\sigma}{K_\sigma^*} = \frac{K_\tau}{K_\tau^*} \tag{5}$$

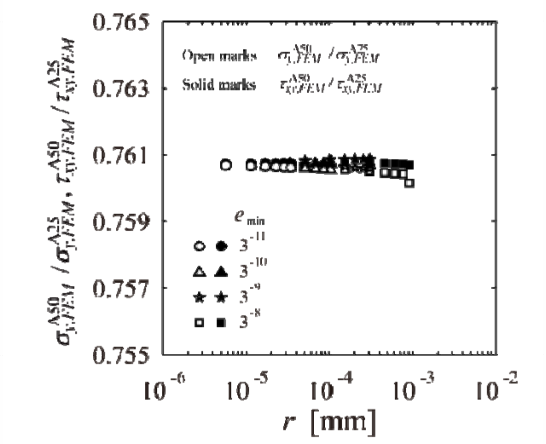

Figure 5 Relationship between $\sigma_{y,FEM}^{\mathrm{A50}} \big/ \sigma_{y,FEM}^{\mathrm{A25}}$, $\tau_{xy,FEM}^{\mathrm{A50}} \big/ \tau_{xy,FEM}^{\mathrm{A25}}$ and r when σ_0 = 1MPa

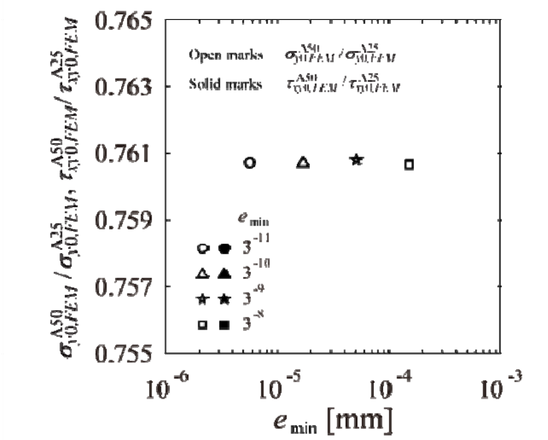

Figure 6 Relationship between $\sigma_{y0,FEM}^{\mathrm{A50}} \big/ \sigma_{y0,FEM}^{\mathrm{A25}}$, $\tau_{xy0,FEM}^{\mathrm{A50}} \big/ \tau_{xy0,FEM}^{\mathrm{A25}}$ and $e_{\min}$ when σ_0 = 1MPa

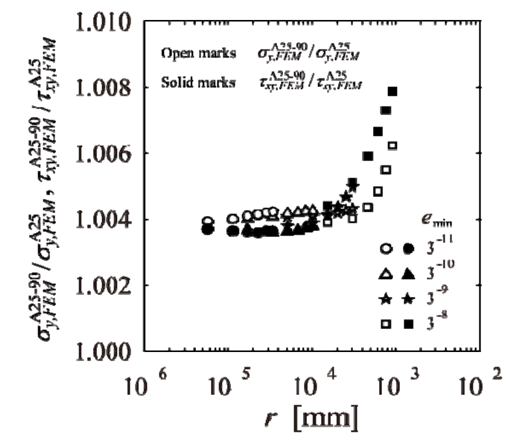

Figure 7 Relationship between $\sigma_{y,FEM}^{\mathrm{A25\text{–}90}} \big/ \sigma_{y,FEM}^{\mathrm{A25}}$, $\tau_{xy,FEM}^{\mathrm{A25\text{-}90}} \big/ \tau_{xy,FEM}^{\mathrm{A25}}$ and r when σ_0 = 1MPa

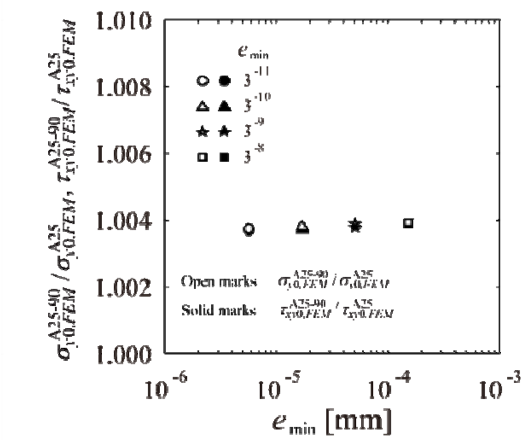

Figure 8 Relationship between $\sigma_{y0,FEM}^{\mathrm{A25\text{-}90}} \big/ \sigma_{y0,FEM}^{\mathrm{A25}}$, $\tau_{xy0,FEM}^{\mathrm{A25\text{-}90}} \big/ \tau_{xy0,FEM}^{\mathrm{A25}}$ and $e_{\min}$ when σ_0 = 1MPa

4. Debonding fracture criterion based on the intensity of singular stress field

Figure 9 shows the relation between $K_\sigma|_{P=1} \big/ K_\sigma^{\mathrm{A25}}|_{P=1}$ and l_2, where $K_\sigma|_{P=1}$ is the intensity of the singular stress field under P = 1N, and $K_\sigma^{\mathrm{A25}}|_{P=1}$ is the $K_\sigma|_{P=1}$ of the specimen A25. When the l_2 is larger than 15mm, the $K_\sigma|_{P=1}$ tends to decrease. Figure 10 shows the relation between $K_{\sigma c} \big/ K_{\sigma c}^{\mathrm{A25}}$ and l_2, where $K_{\sigma c}$ is the intensity of the singular stress field under $P = P_{af}$, and $K_{\sigma c}^{\mathrm{A25}}$ is the $K_{\sigma c}$ of the specimen A25. When the l_2 is smaller than 15mm, the $K_{\sigma c} \big/ K_{\sigma c}^{\mathrm{A25}}$ tends to increase. However, when the l_2 is larger than 15mm, the $K_{\sigma c} \big/ K_{\sigma c}^{\mathrm{A25}}$ becomes constant irrelevant to the l_2. That is because the fracture mode changed from the cohesive fracture to the adhesive fracture. It is confirmed that the solid line is the average of $K_{\sigma c} \big/ K_{\sigma c}^{\mathrm{A25}}$ of all specimens except for specimens A10 and A15. The open circle marks are distributed near the solid line within about 10% error.

Figure 11 shows the relation between $K_\sigma|_{P=1} \big/ K_\sigma^{\mathrm{A25}}|_{P=1}$ and t_2. When the t_2 is larger than 45mm, the $K_\sigma|_{P=1} \big/ K_\sigma^{\mathrm{A25}}|_{P=1}$ almost becomes constant. Figure 12 shows the relation between

$K_{\sigma c}/K_{\sigma c}^{\mathrm{A25}}$ and t_2. The $K_{\sigma c}/K_{\sigma c}^{\mathrm{A25}}$ values are distributed near the solid line within about 10% error.

Figure 13 shows the $K_{\sigma c}/K_{\sigma c}^{\mathrm{A25}}$ values. The average of $K_{\sigma c}/K_{\sigma c}^{\mathrm{A25}}$ values was about 0.997. The $K_{\sigma c}/K_{\sigma c}^{\mathrm{A25}}$ values are distributed near the solid line within about 10% error independent of the l_2 and t_2. It is concluded that the debonding criterion for all types of SLJs having different adhesive thickness and overlap length can be described by the critical intensity of singular stress field $K_{\sigma c}$ = constant.

5. Conclusion

In this study, the debonding fracture criterion for the SLJ having various adhesive length and overlap length was examined. It is found that the singular stress field at the edge corner can be expressed with the same formula even if the adhesive length and overlap length are different. Then when the overlap length is short enough, the fracture criterion can be expressed with the average shear stress at the fracture; when the overlap length is longer than a certain length, the criterion can be expressed with the critical intensity of the singular stress field.

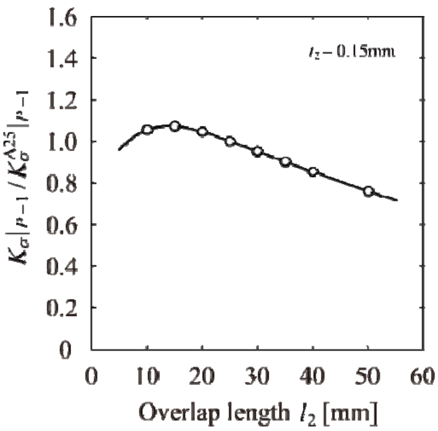

Figure 9 Relationship between $K_\sigma|_{P=1}/K_\sigma^{\mathrm{A25}}|_{P=1}$ and l_2 when P = 1N

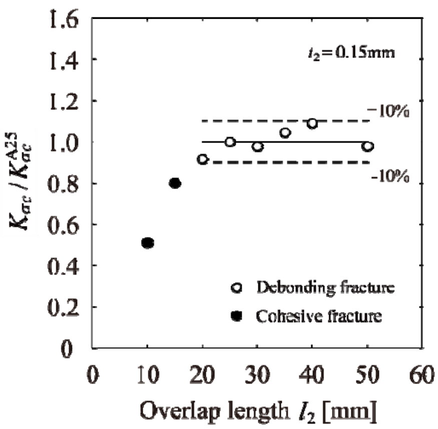

Figure 10 Relationship between $K_{\sigma c}/K_{\sigma c}^{\mathrm{A25}}$ and l_2

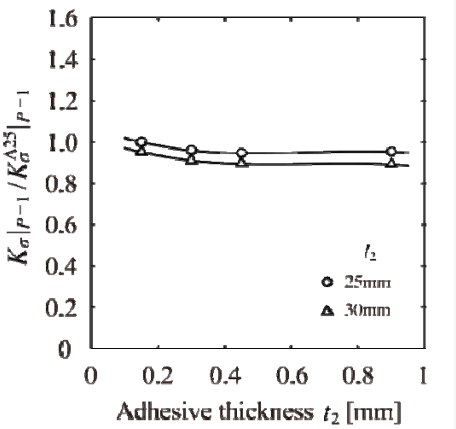

Figure 11 Relationship between $K_\sigma|_{P=1}/K_\sigma^{\mathrm{A25}}|_{P=1}$ and t_2 when P = 1N

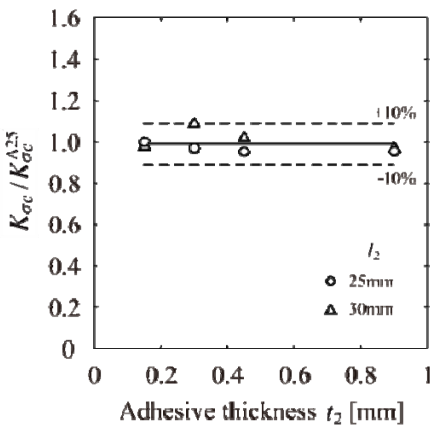

Figure 12 Relationship between $K_{\sigma c}/K_{\sigma c}^{\mathrm{A25}}$ and t_2

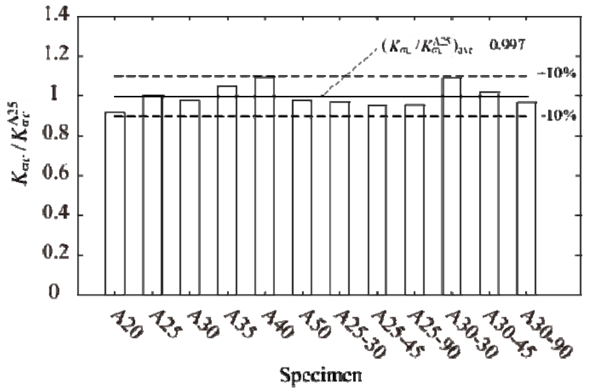

Figure 13 Comparison between $K_{\sigma c} \big/ K_{\sigma c}^{\mathrm{A25}}$ values

References

[1] M. Yasuda, *Hitachi Chemical Technical Report*, No. 40 (2003), pp. 7-12 (in Japanese).

[2] M. Nakamura, *Panasonic Technical Journal*, Vol. 56, No. 4 (2008), pp. 9-16 (in Japanese).

[3] T. Shibuya, *Journal of Japan Institute of Electronics Packaging*, Vol. 7, No. 7 (2008), pp. 9-16 (in Japanese).

[4] M. Shiratori, *Trans. JSME*, Vol. 60, No. 577, Series A (1994), pp. 1905-1912 (in Japanese).

[5] R. Yuuki, *Mechanics of Interface*, Baifukan, (1993) , Tokyo.

[6] Y. Suzuki, *JSME International Journal*, Vol. 30， No. 265 (1987), pp. 1042-1051.

[7] N. -A. Noda, T. Miyazaki, K. Oda, *Proceedings of 3rd ACMFMS*, (2012), pp. 813.

[8] Z. Qian, A. R. Akisanya, *Acta Materialia*, Vol. 46, No. 14 (1998), pp. 4895 – 4904.

[9] A. Mintzas, D. Nowell, *Eng. Fract. Mech.*, 80 (2012), pp. 13 – 27.

[10] J. -H. Park, J. -H. Choi, J. -H. Kweon, *Composite Structures*, Vol. 92 (2010), pp. 2226-2235.

[11] H. Kyogoku, T. Sugibayashi, K. Ikegami, *Trans. JSME*, Vol. 52, No. 476, Series A (1986), pp. 1050-1057 (in Japanese).

[12] K. Nono, T. Nagahiro, *Trans. JSME*, Vol. 52, No. 479, Series A (1986), pp. 1698-1707 (in Japanese).

[13] N.-A. Noda, Y. Zhang, K. -T. Takaishi, X. Lan, *Trans. JSME*, Vol. 78, No. 789, Series A (2011), pp. 651-655 (in Japanese).